J. Synchrotron Rad. (1996). **3**, 53–61

Development of a Two-Dimensionally Tunable Focusing Monochromator for Protein Crystallography at High-Energy Undulator Beamlines

Yoshiaki Kawano† and Nobuo Kamiya*

SPring-8 Project Team, The Institute of Physical and Chemical Research (RIKEN), Hirosawa 2-1, Wako, Saitama 351-01, Japan

(Received 5 October 1995; accepted 2 January 1996)

A two-dimensionally tunable focusing monochromator has been developed for protein crystallography at high-energy undulator beamlines of third-generation synchrotron radiation facilities. This monochromator consists of a silicon wafer fabricated with an oblique-cut angle between the Bragg net plane and the crystal surface, and adhered onto a table-like copper block. The radii of curvatures are altered independently in two directions by expanding the spaces between the table legs. The versatilities of the meridional and sagittal curvatures were confirmed by X-ray experiments and three-dimensional shape measurements, respectively. The two-dimensional focusing ability was demonstrated using high-energy X-rays of 37.7 keV emitted from a bending-magnet source at the Photon Factory. A quasi-isotropic profile of converged X-rays was achieved near the focal position. The apparent gain of photon flux was 21. As a result of these excellent monochromator characteristics, a diffraction pattern of a hen egg-white lysozyme crystal was successfully obtained using high-energy X-rays.

Keywords: monochromators tunable at high energy; two-dimensional focusing; protein crystallography; high-energy undulators.

1. Introduction

Protein crystal structure analysis is a powerful tool for revealing the three-dimensional structures of biological macromolecules at atomic resolution. In order to collect reflection data rapidly from the sample crystals and to resolve phase problems using anomalous-dispersion effects, synchrotron radiation with high intensity and a wide range of accessible energies is very useful in protein crystallography (Helliwell, 1992). In second-generation synchrotron radiation facilities, however, X-ray energies applicable to protein crystallography have been limited to below 20 keV since the bending magnets in these facilities generate X-rays with a sufficiently high flux only at energies below 20 keV.

In this respect, undulators (Attwood, Halbach & Kim, 1985) installed in third-generation synchrotron radiation facilities (Buras & Materlik, 1986; Shenoy & Moncton, 1988; JAERI-RIKEN SPring-8 Project Team, 1991) have drawn much of the attention of protein crystallographers. These undulators are capable of emitting highly brilliant, low-divergence and quasi-monochromatic X-rays, practically meeting all the conditions set for X-ray sources in protein crystallography. In third-generation facilities, especially in SPring-8, high-brilliance X-ray beams will be available in a wide energy range of 6–40 keV from a vacuum-sealed undulator, the 'in-vacuum undulator' (Yamamoto *et al.*, 1992), having fundamental and third-harmonic emissions.

High-intensity X-ray beams in the high-energy region between 20 and 40 keV, which are not available in second-generation facilities, are desirable in protein crystallography since crystal absorption errors are essentially eliminated (Helliwell, Ealick, Doing, Irving & Szebenyi, 1993) and the accessible elemental absorption edges are elongated to the *K* edges of biologically useful molybdenum, cadmium, iodine and xenon, and the *L* edges of uranium.

Furthermore, high-energy X-rays around 38 keV are indispensable for collecting ultra-high-resolution data (Deacon *et al.*, 1995) using X-ray detectors such as charge-coupled-device (CCD) cameras and imaging plates (IPs) including their readout apparatus. These detectors are highly sensitive to 38 keV X-rays because the *K* edges of caesium and barium, which are the major components in the phosphors of CCD cameras and IPs, respectively, exist near this energy value.

Although undulator X-rays have a small beam size because of their low-divergence nature, the cross-sectional areas of the beams will be much larger than the size of protein crystals at the sample position because of the large radii of storage rings in third-generation facilities. Undulator beams with a relatively narrow bandpass of 10^{-2} must be further monochromatized to a bandpass of less than 10^{-3} for protein crystallography. One of the major problems hindering the effective use of undulator beams

† Division of Biological Sciences, Graduate School of Science, Hokkaido University, Sapporo 060, Japan.

of 20–40 keV in protein crystallography was therefore considered to be the lack of a focusing monochromator which can two-dimensionally converge low-divergence and high-energy X-rays with high intensity onto the samples.

There are two types of focusing monochromators commonly utilized for protein crystallography in second-generation facilities: triangular bending monochromators (Lemonnier, Fourme, Rousseaux & Kahn, 1978) and 'sagittal focusing' monochromators (Sparks, Borie & Hastings, 1980; Matsushita, Ishikawa & Oyanagi, 1986; Pascarelli *et al.*, 1996). The triangular bending monochromator is usually fabricated with an oblique-cut angle between the Bragg net plane and the monochromator surface for realizing a large demagnification ratio, and is usually used in a horizontal dispersion geometry. In contrast, the two crystals in the sagittal focusing monochromator are set in a vertical dispersion geometry. Owing to these geometrical differences coupled with an asymmetry of synchrotron radiation source sizes in both directions, the triangular bending monochromator is considered to have a higher throughput or a wider bandpass than the sagittal focusing monochromator.

With regard to focusing abilities, the triangular bending monochromator can easily realize a cylindrical surface in one dimension, yet it must be combined with another focusing element such as total reflection mirrors in order to realize two-dimensional focusing (Helliwell *et al.*, 1982). The sagittal focusing monochromator is, in general, used to obtain a pseudo two-dimensional focal point. However, its application to undulator X-ray beams is considered to be difficult since the size of the undulator beams is too small for convergence using sagittal focusing geometry.

There are also various types of two-dimensional focusing monochromators that have been fabricated so far with lithium fluoride (Sakabe, 1983), germanium (Wittry & Golijanin, 1988), quartz (Berreman, Stamatoff & Kennedy, 1977; Förster, Gäbel & Uschmann, 1992) and silicon crystals (Kawata, Sato, Higashi & Yamaoka, 1994) by simultaneous bending in two directions. None of these, however, have any tunability in the X-ray energy range. Since tunability is an indispensable function of the monochromators used in protein crystallography, these monochromators cannot accommodate the present purpose.

It is clear that reliable two-dimensionally tunable focusing monochromators must be developed in the horizontal dispersion geometry with oblique-cut angles in order to effectively utilize high-energy X-ray beams with high intensity that are extracted from the undulator beamlines in the third-generation facilities. In this paper we describe the performance of a newly developed two-dimensionally tunable focusing monochromator, confirmed by experiments conducted in a laboratory and those at beamline 15B of the Photon Factory (Photon Factory Activity Report, Number 4, 1986) of the National Laboratory for High Energy Physics.

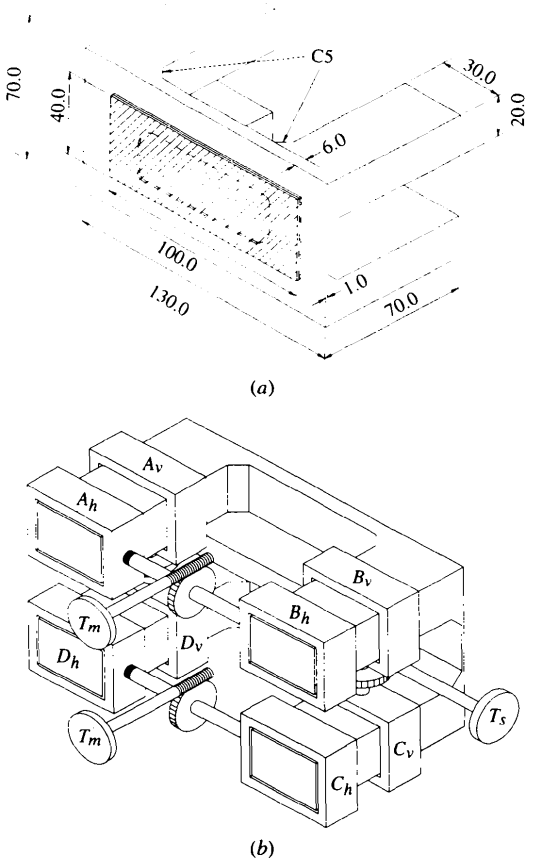

Figure 1
Schematic drawing of the two-dimensionally tunable focusing monochromator. (*a*) Si wafer (hatched) adhered onto a table-like copper block. Dimensions are in millimeters. C5: 5 × 5 mm corner. (*b*) Bending mechanism.

2. Design of a two-dimensionally tunable focusing monochromator

A silicon (111) wafer of area 40 × 100 mm and thickness 0.5 mm was fabricated by Sharan Instruments Company Ltd with an oblique-cut angle between the Bragg net plane and the crystal surface, and adhered onto a table-like copper block, as shown in Fig. 1(*a*). A hillock of 0.5 mm height with a 25 × 70 mm hollow in the centre was made on the table surface, and the silicon wafer was adhered onto the copper block with epoxy glue on top of the hillock.

The radii of curvatures in the meridional and the sagittal directions of the silicon wafer were changed independently by rotating four screws (two pairs each of T_m and T_s) in a special bender, as indicated in Fig. 1(*b*). The bender had eight holders, two holders fixing the horizontal and vertical positions of each leg of the copper table. The horizontal (A_h–D_h) and vertical (A_v–D_v) holders were placed on corresponding cross-roller guides [not shown in Fig. 1(*b*) for clarity], and roller bearings perpendicular to the cross-roller guides were included in the holders in order to reduce possible frictional forces produced during expansions of the space between the legs. The expansions of the spaces would result in alterations of the radii of curvatures.

An asymmetric reflection geometry is commonly used in the meridional direction in many focusing monochromators. With the oblique-cut angle, α, the asymmetry factor (b) can

Table 1
Design parameters of the present two-dimensional focusing monochromator.

Distance from source to monochromator, p (m)	37.0
Distance from monochromator to focus, q (m)	4.47
X-ray energy (keV)	37.7
Bragg angle, θ, of Si (111) (°)	3.008
Oblique-cut angle, α* (°)	−2.36
Asymmetry factor, b*	8.27
Radius of meridional curvature, R_m* (m)	396
Radius of sagittal curvature, R_s* (m)	0.42

* Definitions given in text.

be defined as

$$b = \sin(\theta_B - \alpha)/\sin(\theta_B + \alpha), \quad (1)$$

where θ_B denotes the Bragg angle. Under the Guinier condition, in which both the X-ray source and the focal point are on the Rowland circle, the radius of curvature in the meridional direction (R_m) is

$$R_m = p/\sin(\theta_B - \alpha) = q/\sin(\theta_B + \alpha), \quad (2)$$

where p represents the distance from the light source to the monochromator, and q the distance from the monochromator to the focal point. In adjusting the focal lengths both in the meridional and sagittal directions, the radius of sagittal curvature (R_s) should satisfy

$$R_s = R_m(\sin^2\theta_B - \sin^2\alpha). \quad (3)$$

Table 1 shows the design parameters of the present two-dimensional focusing monochromator (Johann type). These values were determined so as to examine adequately the focusing ability of the monochromator at beamline 15B of the Photon Factory. This beamline is an X-ray branch line from a bending-magnet source for high-speed X-ray topography, where the distance between its source point and the experimental station was as long as that for the SPring-8 undulator beamline.

3. Simulation of a two-dimensionally curved shape

It is well known that anticlastic bending in the meridional direction of the monochromator wafer can be established by sagittally bending the wafer with a small radius of curvature when the wafer has mechanically free edges (Sparks, Ice, Wong & Batterman, 1982). In contrast, no change in the shape of the monochromator under the present two-dimensional bending mechanism was evident at all, since the boundaries of the monochromator were adhered onto the table-like copper block.

In order to evaluate the deviation of the actual surface from the toroidally curved one, the shape of the monochromator surface was simulated by the finite-element method, taking the structural effect of the table-like copper block into consideration. A quarter model of the monochromator was subjected to simulation performed using the software program *ANSYS* of Swanson Analysis Systems Inc. Acceleration due to gravity was not considered in this calculation.

Fig. 2(*a*) shows the simulated trace along the centreline in the meridional direction. Although the overall trace can be regarded approximately as a circle, the detailed structure of the trace near the centre must be carefully examined,

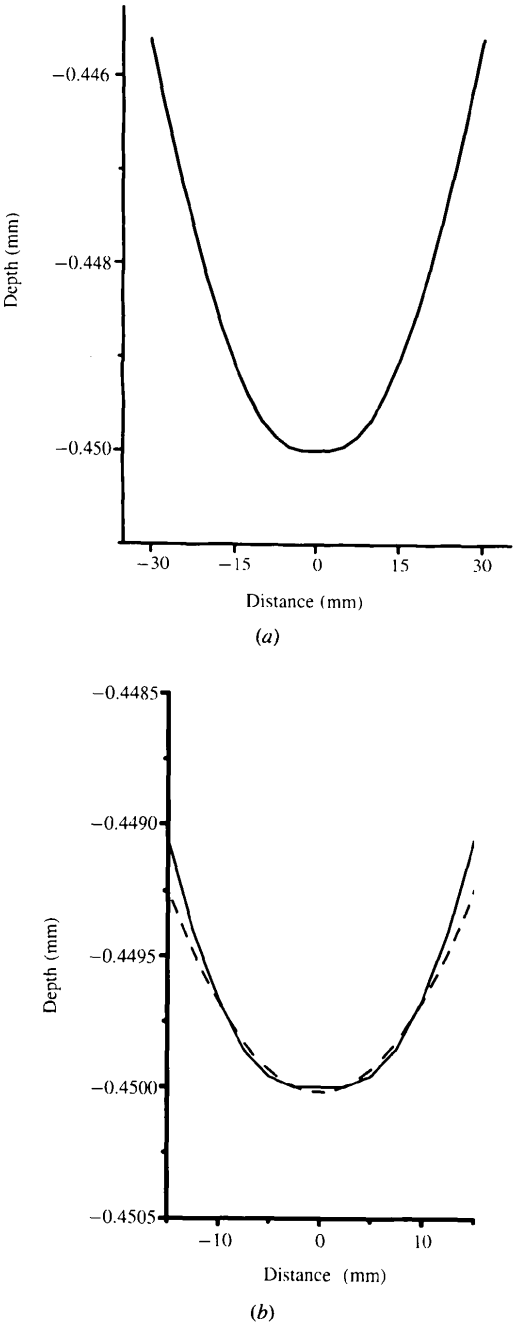

Figure 2
Simulation in the meridional direction. (*a*) The ±30 mm area around the centre, and (*b*) threefold magnification of the ±10 mm area. Continuous line: simulated trace; broken line: least-squares fit of an ideal circle. Distance and depth are measured from the centre and edge of the monochromator wafer, respectively.

since it is the central area (±10 mm) that will be irradiated by the small beam from the undulator. Fig. 2(*b*) displays the central region of Fig. 2(*a*) with a magnification factor of 3. The radius of curvature near the centre is larger than those of adjacent areas. This feature can also be regarded as a pair of bending components, with a smaller radius of curvature than the ideal value, arranged side by side with a small separation.

The deviation of the calculated trace from an ideal circle is, however, very small (within a region of ±10 mm). Using the least-squares method, the root-mean-square deviation (r.m.s.d.) from the ideal circle of 141 m radius (broken line) was calculated to be only 0.051 μm in the present case. On the other hand, as regards the simulated trace in the sagittal direction, no feature such as that observed in the meridional direction was found (data not shown), and the averaged radius of curvature calculated was 1.14 m with an r.m.s.d. of 0.041 μm in the central region of ±1 mm.

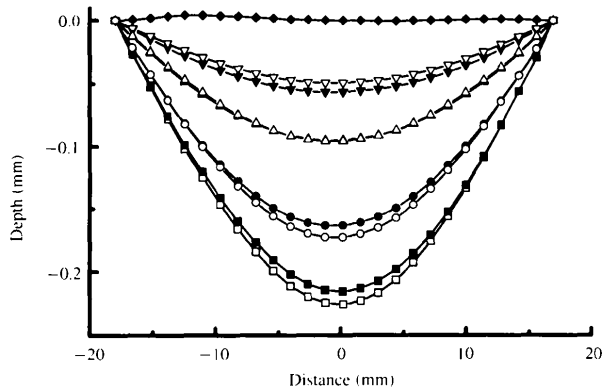

(*a*)

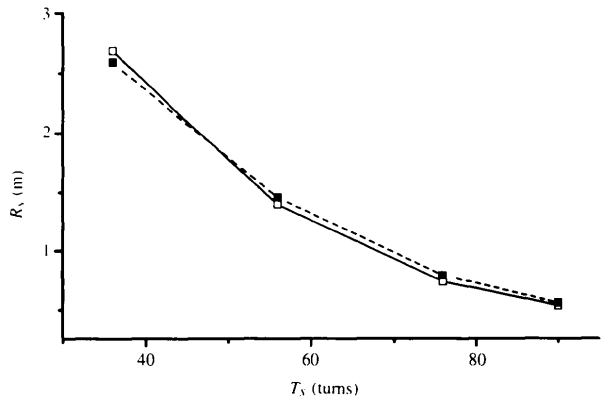

(*b*)

Figure 3
(*a*) Trace and versatility in the sagittal direction. Profile measurements were carried out at 0.01 mm intervals at T_s = 90 (black squares: loosening, white squares: fastening), 76 (black circles, white circles), 56 (black triangles, white triangles), 36 (black inverted triangles, white inverted triangles) and 0 (black diamonds). Each symbol represents one data point selected from every 140 data points for clarity. Distance from the centre and depth from a standard point (18 mm from the centre) are indicated. (*b*) Reproducibility in the radius of sagittal curvature. Black squares: loosening, white squares: fastening.

4. Bending properties and versatility of curvature

The triangular bending monochromator with a large asymmetry factor has frequently been used in beamlines for protein crystallography at second-generation synchrotron radiation facilities. One of the major characteristics of this monochromator is its tunability in a certain range of X-ray energies. The present study is significant in that it produces tunability in the two-dimensional focusing monochromator.

4.1. *Sagittal direction*

As a result of the small radius of sagittal curvature in the present monochromator, the shape and the versatility of the curvature can be precisely measured with a three-dimensional contour measurement machine (MP2000, Raytex Company Ltd). Fig. 3(*a*) shows the observed central profiles of the monochromator in the sagittal direction with several values of T_s rotation, with T_m rotation set to zero. (Hereafter, the rotation numbers for T_s and T_m screws are also denoted by T_s and T_m, respectively.) In

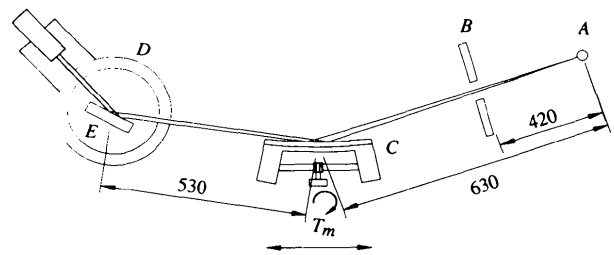

(*a*)

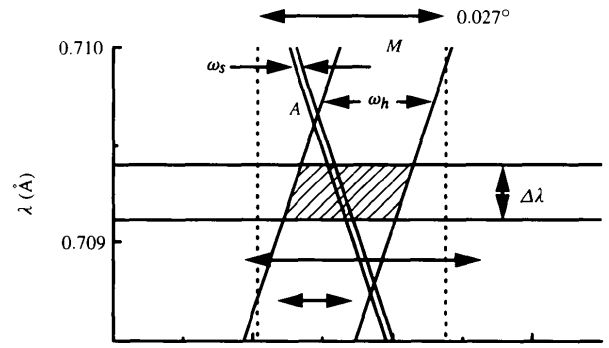

(*b*)

Figure 4
(*a*) Experimental set-up for X-ray measurements. *A*, X-ray source point (0.2 × 0.2 mm); *B*, *XY* slit; *C*, two-dimensional focusing monochromator on a sliding stage; *D*, $\theta/2\theta$ goniometer; *E*, Si crystal analyzer; T_m, meridional bending screw. Distances are expressed in mm. (*b*) DuMond diagram of the X-ray experiments. $\Delta\lambda$, wavelength spread of Mo $K\alpha_1$ radiations; ω_h, angular emergence width of the two-dimensional focusing monochromator in the meridional direction; ω_s, intrinsic width of Bragg reflection of the Si (111) crystal analyzer on a $\theta/2\theta$ goniometer. The domain (*A*) for the analyzer moves following the θ-axis rotation of the goniometer, and that for the monochromator (*M*) shifts its angular position following its translation in the meridional direction. The broken lines indicate the angular width of the incident X-rays on the monochromator.

this measurement, the monochromator was first fully bent to a maximum value of T_s = 90. The averaged radius of curvature near the centre (±1 mm) was calculated to be 0.54 m with an r.m.s.d. of 0.03 μm. The screws were then loosened to T_s = 0 and fastened to T_s = 90. Fig. 3(*b*) clearly shows that the bending mechanism can realize excellent reproducibility in the radius of sagittal curvature of the monochromator.

4.2. *Meridional direction*

The MP2000 apparatus could not measure the central traces in the meridional direction due to the large radii of corresponding curvatures. In order to determine them, an experimental set-up was constructed, as shown in Fig. 4(*a*). After being shaped with a 0.2 (horizontal) × 0.5 mm (vertical) *XY* slit, Mo $K\alpha_1$ X-rays illuminated the present two-dimensional focusing monochromator. Intensity profiles of the X-rays reflected from the monochromator were measured with a silicon (111) crystal analyzer mounted on a $\theta/2\theta$ goniometer (MAC Science Company Ltd) in a (+,+) configuration. The measurements were carried out as a function of T_m while varying the monochromator position in the meridional direction with an interval of 2 mm. Before the measurement, the monochromator was bent in the sagittal direction by T_s = 90.

Fig. 4(*b*) shows a DuMond diagram of this experiment. The Mo $K\alpha_1$ radiation spread over 0.0003 Å in wavelength ($\Delta\lambda/\lambda = 4 \times 10^{-4}$). All of the intensity profiles were measured with angular widths of *ca* 0.012° [see the hatched area in Fig. 4(*b*)] in terms of full width at half maximum (FWHM). The angular width (ω_h) of the monochromator for emergence was estimated to be similar to the observed value since the wavelength spread of Mo $K\alpha_1$ radiation was too small to account for the wide width observed. Considering the asymmetry factor (b = 2.1) under this experimental condition, the angular width (ω_o) of the monochromator for acceptance is calculated to be 0.006°, which is two times larger than the theoretical value for a perfect crystal with an asymmetry factor of 2.1 in the wavelength spread of Mo $K\alpha_1$ radiation. The increase in the angular acceptance width may be due to marked bending of the monochromator with the small radius of sagittal curvature.

The evaluated peak positions are plotted in terms of θ of the $\theta/2\theta$ goniometer (Fig. 5*a*). The peak positions varied linearly with the positional changes of the incident X-rays on the two-dimensionally bent monochromator. This corresponds to the angular variation of the monochromator surface. The observed slope of each line, $\Delta\theta/\Delta x$, is related to the radius of meridional curvature, R_m, by

$$\Delta\theta/\Delta x = 1/R_m. \quad (4)$$

The positive and negative slopes correspond to concave and convex shapes, respectively. The averaged radii of curvatures evaluated by least-squares fit to the straight lines were over 61 m for the concave shapes, and over 110 m for the convex ones. These changes in the curvatures were experimentally confirmed to be reversible, as shown in Fig. 5(*b*). Although the deviations of the R_m values are relatively large at T_m = 0 and −1, they are mainly due to the small values of the corresponding slopes compared with the positional errors of measured intensity profiles.

5. Focusing of high-energy X-rays

The focusing capabilities of the monochromator for high-energy X-rays were carefully examined using beamline 15B at the Photon Factory. Shaped with an *XY* slit having horizontal and vertical opening widths of 1.5 and 1.0 mm, respectively, white X-ray beams were incident on the monochromator mounted on a Huber goniometer. The corresponding energy of the goniometer angle was set to be 37.7 keV, referring to a standard angle for the *K* absorption edge of barium (E = 37.5 keV). Under the focusing conditions of T_s = 90 and T_m = 0, the X-ray beams reflected by the monochromator were recorded on industrial X-ray films (IX80, Fuji Film Company). Five photographs were taken at 2.64, 3.49, 4.11, 4.45 and 4.89 m from the monochromator. The photographs were scanned with a densitometer (Model 1010M Micro-D, Perkin-Elmer

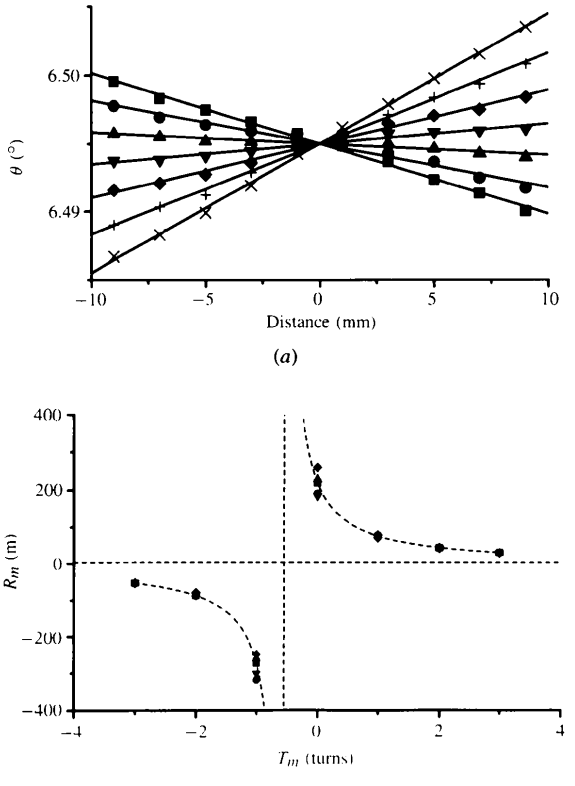

Figure 5
(*a*) Evaluated peak positions plotted in terms of θ and versatility of meridional curvature. T_m = 3 (crosses), 2 (plus signs), 1 (black diamonds), 0 (black inverted triangles), −1 (black triangles), −2 (black circles) and −3 (black squares). Distance represents the positional changes of incident X-rays from the monochromator centre. (*b*) Reproducibility of the radius of meridional curvature in six independent measurements. The horizontal and vertical broken straight lines are asymptotes.

Company), and the horizontal and vertical FWHM beam sizes measured were plotted, as shown in Fig. 6.

The beam size observed in the sagittal direction decreases monotonically without any clear focal points in the given range of distance. It is anticipated that the focal point may be outside the experimental hutch of beamline 15B, so that one can infer that the present condition of T_s = 90 is insufficient for converging X-rays at the same position in the two directions. This inference is consistent with the results reported above that the radius of sagittal curvature of 0.54 m at T_s = 90, determined from the three-dimensional contour measurements, is larger than the expected value of 0.42 m (see Table 1).

On the other hand, the beam size in the meridional direction has a concave feature in the experimental distance ranging from 2.64 to 4.89 m. Assuming a function of the second order, a least-squares fit indicates a focal point at 3.96 m, which is 0.5 m shorter than the designed value of 4.47 m. The estimated minimum focal spot size is 0.22 mm with a focal depth of *ca* ±0.5 m.

Fig. 7 shows the two contour maps of reflected X-rays taken at distances of 2.64 and 4.89 m. In the former, the observed profile includes two peaks in the horizontal direction. This double-peak distribution is observed not only in the former case but also in the two contour maps measured at 3.49 and 4.11 m. The double-peak distribution tends, however, to disappear in the other two contour maps. As shown in Fig. 7(*b*), the X-ray beam, the original extent of which was 1.5 × 1.0 mm, was successfully converged down to 0.22 × 0.27 mm in a quasi-isotropic profile with the present monochromator. The beam profile attained should, however, be considered as an overlap of the two components observed at the shorter distance, as shown in Fig. 7(*a*).

With reference to the beamline specifications, the FWHM source sizes of beamline 15B are reported to be 0.80 (horizontal) and 0.37 mm (vertical) (Photon Factory Activity Report, Number 10, 1992). The expected size of the focal spot is calculated to be 0.10 × 0.04 mm based on the asymmetry factor of 8.27 for the present monochromator. The observed meridional size of the focal point is, however, two times larger than the calculated value. Furthermore, the observed focal length differs from the designed one by 0.5 m, and the estimated focal depth seems to be wider than expected.

These discrepancies can be explained as follows. Based upon the simulations carried out, as well as the observed distribution of the X-ray intensity profiles, it is conceivable

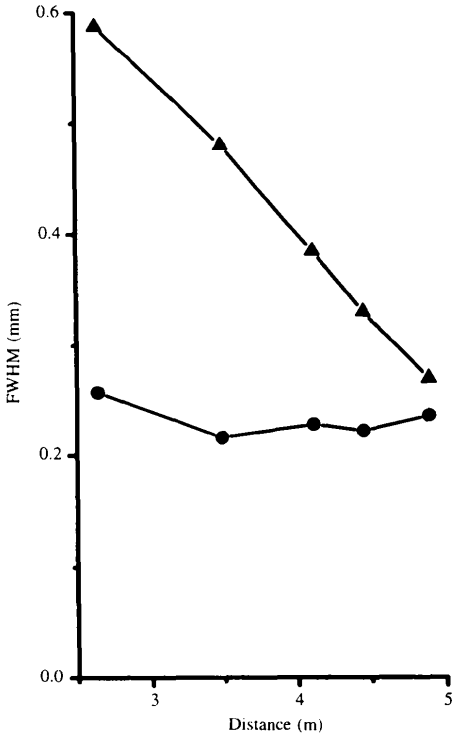

Figure 6
FWHM size of reflected X-rays in the sagittal (black triangles) and meridional (black circles) directions. Distance is measured from the monochromator.

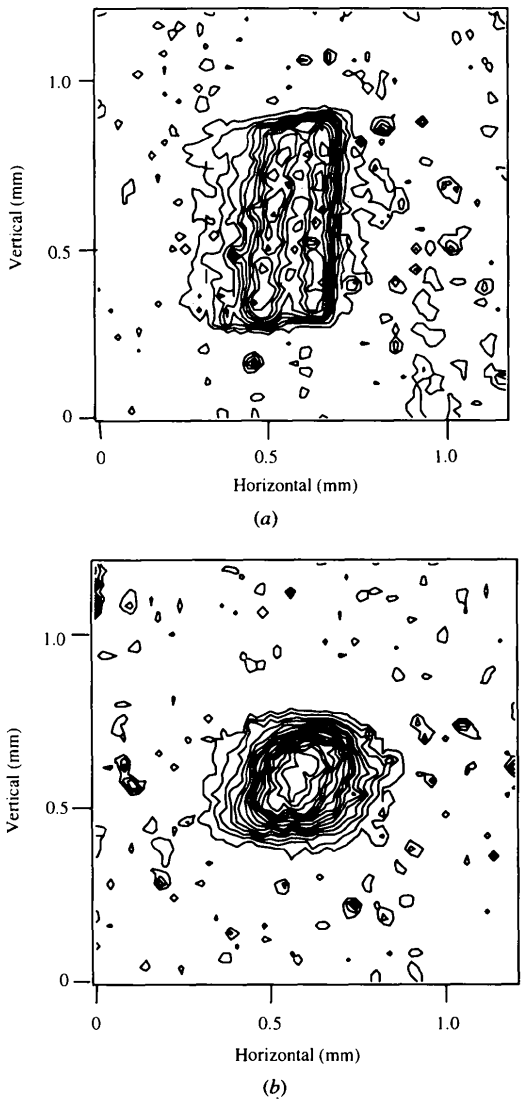

Figure 7
Contour maps of reflected X-rays taken at (*a*) 2.64 m and (*b*) 4.89 m. The contours start from 0.2 optical density with 0.05 intervals.

that the active area of the monochromator surface consists of three parts in the meridional direction: one is the central area which is cylindrical rather than toroidal, and the other two are the toroidal areas adjacent to it. The discrepancies should also be considered in terms of the chromatic aberration of the focusing monochromator with as large an asymmetry factor as in the present case. Applying the formulation recently derived by Takeshita (1995) to the present monochromator, the meridional focal size is calculated to be 0.18 mm when the radii of meridional curvatures are assumed to be 300 m for the two toroidal areas. This implies that the expected focal size in the meridional direction is much larger than the value calculated using only the asymmetry factor of the monochromator.

Fig. 8 illustrates the situations considered above. The double-component properties observed at position *a* are diminished at position *c*. The smallest beam size could be realized at the apparent focal point *b*. This figure also visually explains the findings that the measured focal length is different from the design value, and that the beam size is larger than the expected one. Furthermore, the depth of focus could be broader than that expected with an ideally curved monochromator.

To evaluate the reflectivity and the flux gain of the present two-dimensional focusing monochromator, another set of four photographs were taken after substituting the monochromator with a flat silicon (111) block ($\alpha = -0.70°$, $b = 1.61$), and two photographs taken at 4.89 m, one with the monochromator and the other with the silicon block, were used. The optical density was deduced by integrating the recorded densities over the entire region of the beam area. The ratio of the optical density of the present monochromator to that of the silicon block was 3/5. Since the theoretical ratio of angular widths for acceptance is 1/2 between the present monochromator and the silicon block under the conditions adopted for the focusing experiments, the monochromator developed in this work can be regarded as one which loses no reflectivity in its two-dimensional bending mechanism.

The flux gain evaluated from the peak heights observed in the two photographs was as high as 10. Using the same value of 1/2 as the theoretical ratio of angular widths for acceptance, the flux gain was recalculated to be 21, which was in good agreement with the size demagnification from the incident X-ray beam (1.5 × 1.0 mm) to the focused one (0.22 × 0.27 mm).

As already mentioned, the angular acceptance width of the present monochromator was increased by bending in the sagittal direction. In the above considerations, it is assumed that the reflectivity of the monochromator is reduced following the increase in the angular acceptance width. That is, the integrated intensity of the reflected X-rays with the present monochromator is assumed to be similar to the theoretical value obtained for a perfect crystal.

The energy resolution of the present monochromator has not been measured. However, it is estimated to be 2×10^{-3} under the conditions of the focusing experiments based upon the angular acceptance width of the two-dimensionally bent monochromator, 0.006°.

6. Oscillation photograph of a protein crystal

An oscillation photograph of a tetragonal crystal of hen egg-white lysozyme was taken using the high-energy X-ray beam focused with the monochromator, as shown in Fig. 9. The crystal of size 1.2 × 1.2 × 0.5 mm was mounted on a Huber precession and rotation camera. The *c* axis was set near the spindle axis. The camera was located 4.45 m behind the monochromator, and an imaging plate (BAS-UR, Fuji Film Company) was used for recording the diffraction pattern.

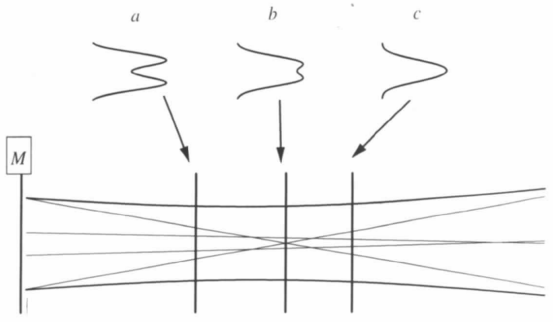

Figure 8
Focusing scheme in the meridional direction. The monochromator (*M*) is represented by a line for clarity. Profiles *a*–*c* are expected at the indicated positions.

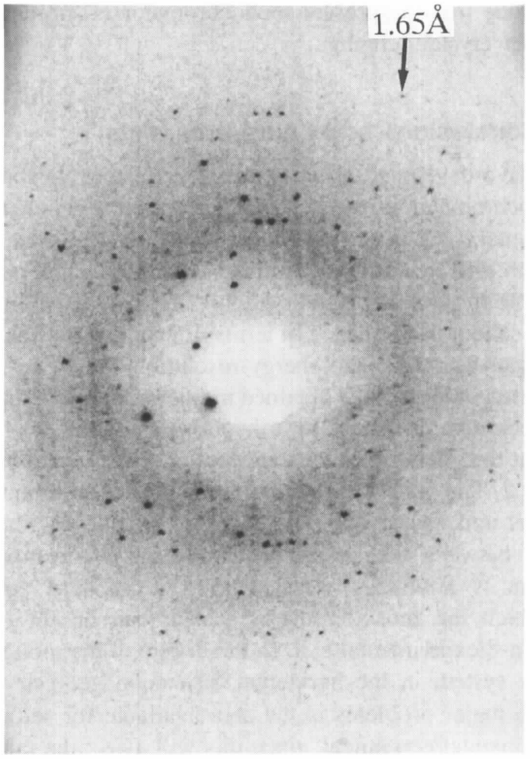

Figure 9
Oscillation photograph of a hen egg-white lysozyme crystal using 37.7 keV X-rays. The sample crystal belongs to a tetragonal system (space group $P4_32_12$) with cell dimensions $a = 79.1$ and $c = 38.0$ Å. The distance from the sample crystal to the imaging plate is 100 mm. The arrow indicates a spot of 1.65 Å resolution.

Table 2
Design parameters for a hypothetical monochromator system.

Distance from source to monochromator, p (m)	36		
Distance from monochromator to focus, q (m)	6–10		
Whole range of X-ray energy (keV)	20–40		
Monochromator	I	II	III
Individual energy range (keV)	20.0–25.3	25.3–31.9	31.9–40.0
Bragg angle (θ) of Si(111) (°)	5.67–4.49	4.49–3.56	3.56–2.83
Oblique-cut angle, α* (°)	−3.21	−2.54	−2.01
Asymmetry factor, b*	3.6–6.0	3.6–6.0	3.6–5.9
Radius of meridional curvature, R_m* (m)	233–269	294–339	371–427
Radius of sagittal curvature, R_s* (m)	1.55–0.81	1.22–0.64	0.97–0.52

* Definitions given in text.

The oscillation angle and the exposure time were 0.1° and 5 min, respectively, at the Photon Factory storage ring current of 290 mA. The relatively long exposure time was required partly because of the low brilliance of the X-ray beam generated by the Photon Factory bending magnet at 37.7 keV and partly because of the small horizontal and vertical acceptances of 41 and 27 μrad of the present monochromator. In order to obtain a diffraction image of good quality with the high-energy X-rays, a well focused and highly monochromatic X-ray beam should be used since the diffraction pattern of the high-energy X-ray beam would be spatially reduced. Since two neighbouring spots were distinctly separated in the horizontal direction with an interval of only 0.87 mm, as shown in Fig. 9, we can conclude that the present monochromator is sufficient for protein crystallography.

7. Conclusions and future prospects

We have developed a two-dimensionally tunable focusing monochromator in the horizontal dispersion geometry for high-energy X-rays from undulators of third-generation synchrotron radiation facilities. This monochromator is suitable for protein crystallography due to its tunability and its excellent performance in terms of small focus size, high flux gain and adequate energy resolution.

Based on the results obtained in this work, we designed a monochromator system for a hypothetical undulator beamline at the SPring-8, the parameters of which are shown in Table 2. The system consists of three individual monochromators and covers the energy range 20–40 keV. The distance between the source point and the monochromator system is arbitrarily selected from a standard position at which the monochromator system can be set in the SPring-8 experimental hall. In the design of the monochromator system in the horizontal dispersion geometry, one of the major problems is the area available for setting up experimental equipment, since this will affect the range of acceptable focusing distances. Considering the conditions of the SPring-8 experimental hall, we choose 6–10 m as the distances between the monochromator system and the focal points while suppressing tangential distances of the focal points from the beamline to less than 1.6 m.

In order to realize the monochromator system for use with the SPring-8 beamline, counter-measures must be taken to cope with the high heat-load problem. The cryogenic cooling techniques developed for the European Synchrotron Radiation Facility may be very powerful. There are two possibilities for utilizing those techniques in our two-dimensionally tunable focusing monochromator: indirect cooling of a very thin wafer or direct cooling of a relatively thick one, as described in this paper. In the former, the thin wafer is fabricated as one body on a table-like silicon block (Rogers *et al.*, 1995) and liquid nitrogen flows through paths drilled in the table legs. In the latter, the relatively thick wafer and the table-like silicon block with the liquid nitrogen paths are individually prepared, then adhered (Yamaoka, Freund, Ohtomo & Krumrey, 1995). For adhesion, however, the epoxy glue used in this study is not applicable because of its poor resistance to synchrotron radiation.

Although these ideas must be simulated by the finite-element method using the *ANSYS* program from the viewpoints of bending properties and heat-load problems, we believe that the final two-dimensionally tunable focusing monochromators may actually be applicable to the SPring-8 undulator beamlines.

The authors acknowledge Drs H. Yamaoka and T. Uruga, and Mr S. Munekawa of RIKEN for their support in experiments, and Dr M. Suzuki for reading the manuscript. They are also grateful to Drs H. Iwasaki and T. Ueki of RIKEN for their encouragement. They also thank the staff of the Photon Factory, in particular, Professor H. Kawata for useful discussions on the two-dimensional focusing monochromators, and Professor N. Sakabe for his kind gift of the BAS-UR imaging plate. This work was supported by the R&D programs of the SPring-8 Project Team.

References

Attwood, D., Halbach, K. & Kim, K. (1985). *Science*, **228**, 1265–1272.
Berreman, D. W., Stamatoff, J. & Kennedy, S. J. (1977). *Appl. Opt.* **16**, 2081–2085.

Buras, B. & Materlik, G. (1986). *Nucl. Instrum. Methods*, A**246**, 21–31.

Deacon, A., Habash, J., Harrop, S. J., Helliwell, J. R., Hunter, W. N., Leonard, G. A., Peterson, M., Hadener, A., Kalb (Gilboa), A. J., Allinson, N. M., Castelli, C., Moon, K., McSweeney, S., Gonzalez, A., Thompson, A. W., Ealick, S., Szebenyi, D. M. & Walter, R. (1995). *Rev. Sci. Instrum.* **66**, 1287–1292.

Förster, E., Gäbel, K. & Uschmann, I. (1992). *Rev. Sci. Instrum.* **63**, 5012–5016.

Helliwell, J. R. (1992). *Macromolecular Crystallography with Synchrotron Radiation*. University of Cambridge, England.

Helliwell, J. R., Ealick, S., Doing, P., Irving, T. & Szebenyi, M. (1993) *Acta Cryst.* D**49**, 120–128.

Helliwell, J. R., Greenhough, T. J., Carr, P. D., Rule, S. A., Moore, P. R., Thompson, A. W. & Worgan, J. S. (1982). *J. Phys. E.* **15**, 1363–1372.

JAERI-RIKEN SPring-8 Project Team (1991). *SPring-8 Project.* Part I. *Facility Design*. JAERI-RIKEN SPring-8 Project Team, The Institute of Physical and Chemical Research, Hirosawa 2-1, Wako, Saitama 351-01, Japan.

Kawata, H., Sato, M., Higashi, Y. & Yamaoka, H. (1994). Photon Factory Activity Report, Number 12. Photon Factory, Tsukuba, Ibaraki 305, Japan. In the press.

Lemonnier, M., Fourme, R., Rousseaux, F. & Kahn, R. (1978). *Nucl. Instrum. Methods*, **152**, 173–177.

Matsushita, T., Ishikawa, T. & Oyanagi, H. (1986). *Nucl. Instrum. Methods*, A**246**, 377–379.

Pascarelli, S., Boscherini, F., Acapito, F. D., Hrdy, J., Meneghini, C. & Mobilio, S. (1996). *J. Synchrotron Rad.* In preparation.

Photon Factory Activity Report, Number 4 (1986). p. 92. Photon Factory, Tsukuba, Ibaraki 305, Japan.

Photon Factory Activity Report, Number 10 (1992). p. R-30. Photon Factory, Tsukuba, Ibaraki 305, Japan.

Rogers, C. S., Mills, D. M., Lee, W.-K., Knapp, G. S., Homberg, J., Freund, A., Wulff, M., Rossat, M., Hanfland, M. & Yamaoka, H. (1995). *Rev. Sci. Instrum.* **66**, 3493–3499.

Sakabe, N. (1983). *J. Appl. Cryst.* **16**, 542–547.

Shenoy, G. K. & Moncton, D. E. (1988). *Nucl. Instrum. Methods*, A**266**, 38–43.

Sparks, C. J., Borie, B. S. & Hastings, J. B. (1980). *Nucl. Instrum. Methods*, **172**, 237–242.

Sparks, C. J., Ice, G. E., Wong, J. & Batterman, B. W. (1982). *Nucl. Instrum. Methods*, **194**, 73–78.

Takeshita, K. (1995). *Rev. Sci. Instrum.* **66**, 2238–2240.

Wittry, D. B. & Golijanin, D. M. (1988). *Appl. Phys. Lett.* **52**, 1381–1382.

Yamamoto, S., Shioya, T., Hara, H., Kitamura, H., Zhang, X., Mochizuki, T., Sugiyama, H. & Ando, M. (1992). *Rev. Sci. Instrum.* **63**, 400–403.

Yamaoka, H., Freund, A. K., Ohtomo, K. & Krumrey, M. (1995). *Rev. Sci. Instrum.* **66**, 2092–2094.